http://doi.org/10.7427/DDI.25.14

14. Integration of geospatial data for mapping variation of sediment thickness in the North Sea

LEMENKOVA Polina*

[1*]Ocean University of China, College of Marine Geo-sciences. 238 Songling Road, Laoshan, 266100, Qingdao, China. ORCiD ID: 0000-0002-5759-1089.

**Address of author responsible for correspondence: Ocean University of China, College of Marine Geo-sciences, e-mail: pauline.lemenkova@gmail.com*

Abstract: The study presents geospatial analysis of the seabed distribution of North Sea sediments. Data include thematic datasets with a high-resolution: GlobSed 5-arc-minute total sediment thickness grid combined with GEBCO regional bathymetric grid and geophysical grids showing EGM2008 geoid undulations and marine free-air gravity. The data have been processed using GMT. The data analysis revealed variations in the occurrence and distribution of sediment materials as well as its relationship with topography and regional geophysical settings, marine free-air gravity and geoid. Analysis of the topographic map was performed to describe the structural features of the seafloor. Ridges, large-scale sandbanks, shallow coastal areas and local depressions illustrate uneven bathymetry with northward increasing depths. The highest recorded value is 12,779.642 m located in the northern ares in the SW coast of Norway. Moderate values of sediment thickness (5,000-6,000 m) stretching in NW direction clearly correlate with the marine gravity anomaly isolines with values 10-20 mGal which points at the local relief forms in central basin of the North Sea. The subsidence of the outer shelf of the North Sea and increase of sediment thickness is notable in the central depressions and northern areas: Faroe Islands and Rockall Plateau. The sediment thickness shows the relationship with the topography increasing toward high latitudes. It is also associated with the isostatic sink of the submarine relief in the peripheral areas of the Arctic Ocean. Topographic compensation for the seafloor subsidence by increasing sediment thickness explains local dislocations connected with submarine geomorphology. This study also demonstrated that accurate GMT-based cartographic visualization of the oceanic seafloor using high-resolution multi-source raster grids is crucial to better understand spatial distribution of the marine sediments in the northern latitudes of the North Atlantic Ocean.
Key words: North Sea, Sediment Thickness, Cartography, Geology, GMT.

INTRODUCTION

Processes of the terrigenous sedimentation are caused by the transfer of the materials from the adjacent land including transportation, deposition and dislocation of the sediment materials. The origin of the deep-sea sedimentation is diverse. Generally, apart from the sediments from the rivers, the material goes to the oceans through glaciers melting and deposits transferred to the seafloor, dust moved by the aeolian processes and storms (Lemenkova, 2019a). The complexity of the ways sediments come in to the sea basin can be illustrated by the transportation pattern. Normally, the glaciomarine sediments from the shelf and transferred by rivers are deposited within the sublittoral areas, and rarely reach deeper regions of the continental slope and abyssal basins. Nevertheless, shelf-deposited sediments may move to the deeper parts of the sea due to the gravitational flows from the shelf edge downwards, avalanche sedimentation, caused by gravity effects.

Previous studies were conducted in the North Sea to understand its geological parameters. These studies were focused on distribution of oil deposits, configuration and dynamics of the Scandinavian and British ice sheets, analysis of the buried tunnel valleys through which sediments are being transported, applying different methods like filters and transformations to potential field data modelling of the crystalline crust, seismic stratigraphy mapping, suspended particulate matter concentration (Johnson et al. 1986; Lyngsie et al. 2006; Van der Molen A. S. 2004; Fettweis et al. 2012). However, only a few studies have focused on sediment distribution over the North Sea area (e.g. Ottesen et al. 2020, 2018; de Haas et al. 1997; Lekens et al. 2009; Lindgreen and Jakobsen, 2012; Alappat et al. 2010), and none of them were based on the GMT scripting techniques.

To be able to better analyze the correlation between the origin, transport, dispersal and spatial variability of sedimentation of the North Sea, it is important to have multi-source datasets processed by the advanced cartographic methods such as GMT, showing geophysical and geological grids of the study area. A large data pool enables to perform an analysis which requires turning to historical data (e.g. sedimentation in the North Sea during last 50-70 years) and recent geophysical fields of the basin area as high resolution grids. Open source data archives were used in this research which have provided evidence of variability of the sediment distribution in context of regional settings of the North Sea. A brief description of the geological and geomorphic settings of the North Sea seafloor introduces its regional settings for better understanding of the specifics of the sedimentation processes.

The distribution of the suspended particulate matter along the coasts of the North Sea varies between individual stations ranging on average from 0.04 to 0.56 g/l (Hache et al. 2019). Among the most important factors they mention the proximity to tidal channels, the adjacent land reclamation areas and harsh weather conditions and inundation events. The highest concentrations of the suspended matter in the North Sea are recorded in the Bay of Kiel (2-4 mg/l) and at the mouth of the Elbe (4-6.9 mg/l). In the SW part of the North Sea, the concentration of the suspended matter does not exceed 1–1.6 mg/l (Krey, 1961).

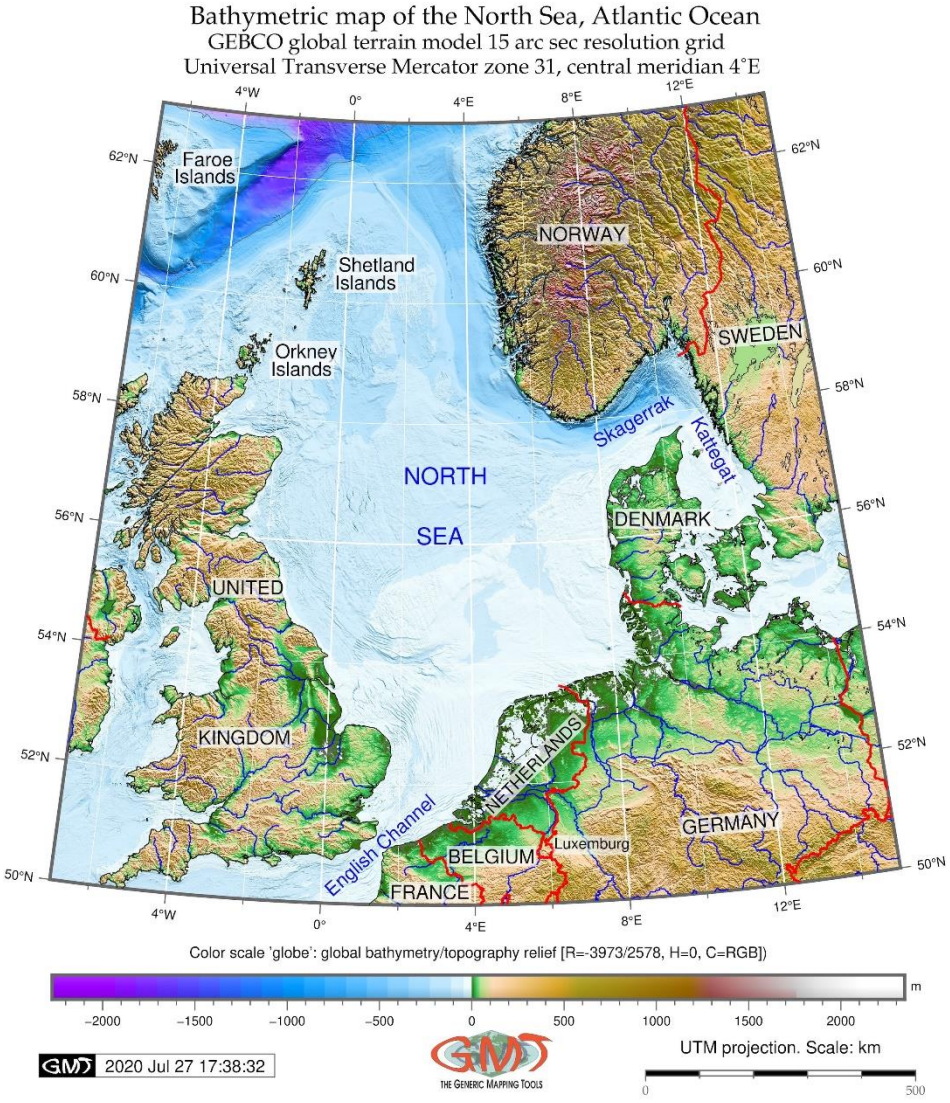

Figure 1. Topographic map of the North Sea basin. Source: author.

Historical sediment records and suspended particulate matter samples in the south-west North Sea were analyzed by Vandermarken et al. (2018) who reported a decrease in dioxin-like compound concentrations in the coastal area and the estuary of the Scheldt River basin and the North Sea coast and the highest bioanalytical equivalent concentrations in the Antwerp harbor. The southern part of the

North Sea is covered by the Quaternary and Tertiary sediments and a succession of Cretaceous, Triassic and Permian rocks, overlying Carboniferous sediments which act as potential hydrocarbon source rocks (Heim et al. 2013). The sediments of the Rhine and Elbe are dominated by silt. The content of suspended matter in the Elbe ranges from 8.9 to 55 mg/l. River water concentration has 15-40 mg/l of the suspended matter and when mixing with sea water, it drops to 10-16 mg/l.

In the section from the mouth of the Elbe near Cuxhaven towards the open basin of the North Sea, the content of suspended matter decreases 5 times over several miles (Krey, 1952). Other sources of the sediment income to the North Sea include storm events, as illustrated by Swindles et al (2018). The concentration of the suspended matter in the coastal and shallow areas of the North Sea is about 10–15 mg/l (Banse 1956), with a gradual decrease towards the open sea to 1-0.5 mg/l. The concentration of the suspended matter increases sharply near the Rhine mouth. In the Wadden Sea it decreases from 60–70 to 7–9 mg/l in the direction from the bay to the open sea (Postma, 1961). The average content of suspended matter in the bay is ca. 23 mg/l, and behind the islands in the adjacent parts of the open sea it decreases to ca. 6 mg/l proving rapid sedimentation of the river suspension.

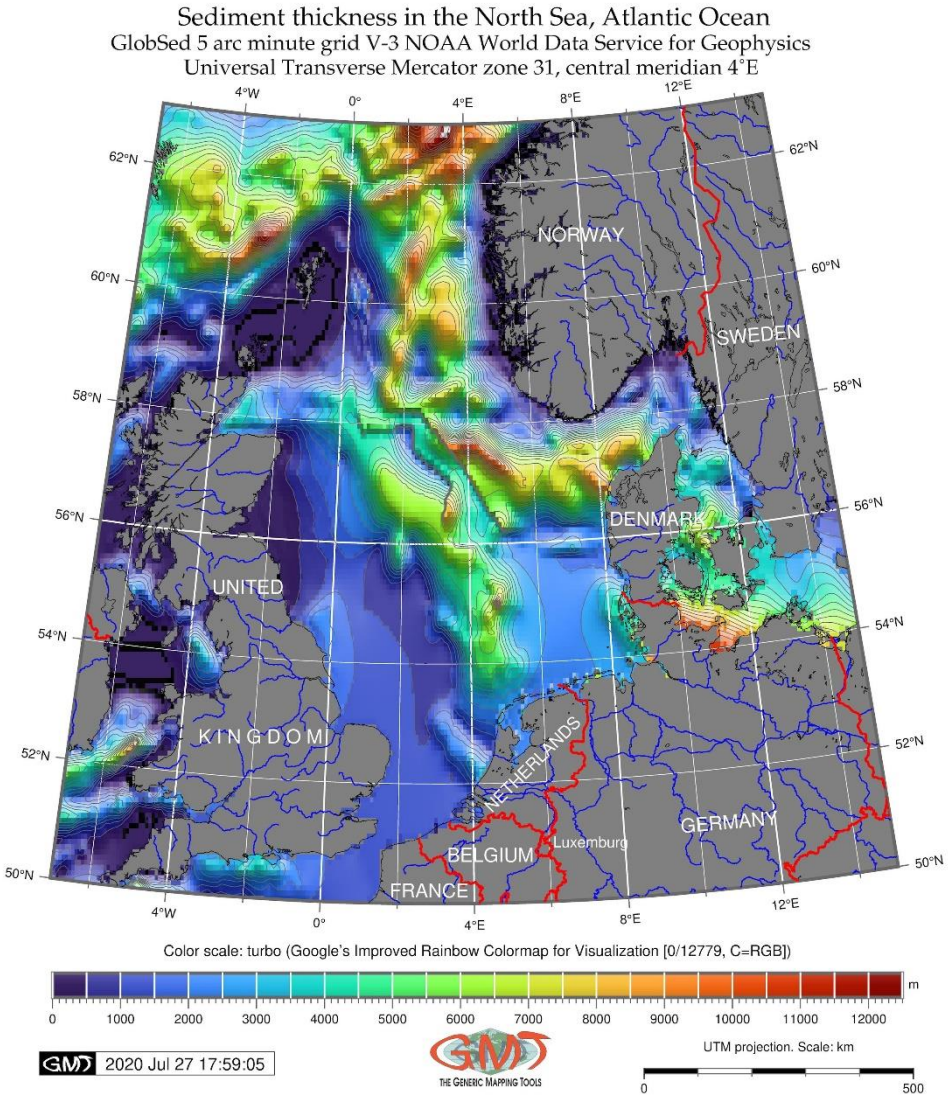

Figure 2. Sediment thickness of the North Sea basin. Source: author.

Southern part of the North Sea is characterized by a sandy bottom with a number of geomorphic landforms formed by sediments: ridges, large-scale sandbanks, local depressions (van Dijk et al. 2012). Such uneven topographic pattern is caused by the strong hydrodynamic changes from water currents (Laban, 2006; Flemming et al. 2017; Visser, 1970). The sediments consist of patches of coarse and mixed sands with a grain size at 250-300 μm (Holtmann and Groenewold, 1994).

MATERIALS AND METHODS

This work has been carried out using multi-source high-resolution datasets. Data accuracy is important for mapping of the marine areas (Smith, 1993; Sadeghi et al. 2019; Lemenkova 2011). Therefore, GEBCO high-quality bathymetry and topography grid with 15-arc second resolution (GEBCO Compilation Group, 2020) was selected for cartographic visualization of the study area (Fig. 1). The sediment thickness (Fig. 2) was based on the GlobSed, a global 5-arc-minute total sediment thickness grid (Straume et al. 2019). The geophysical data of geoid heights (Fig. 3) was mapped based on the EGM2008 2,5 minute resolution grid (Pavlis et al. 2012). The marine free-air gravity anomalies (Fig. 4) were derived from the CryoSat-2 and Jason-1 based grids (Sandwell et al. 2014).

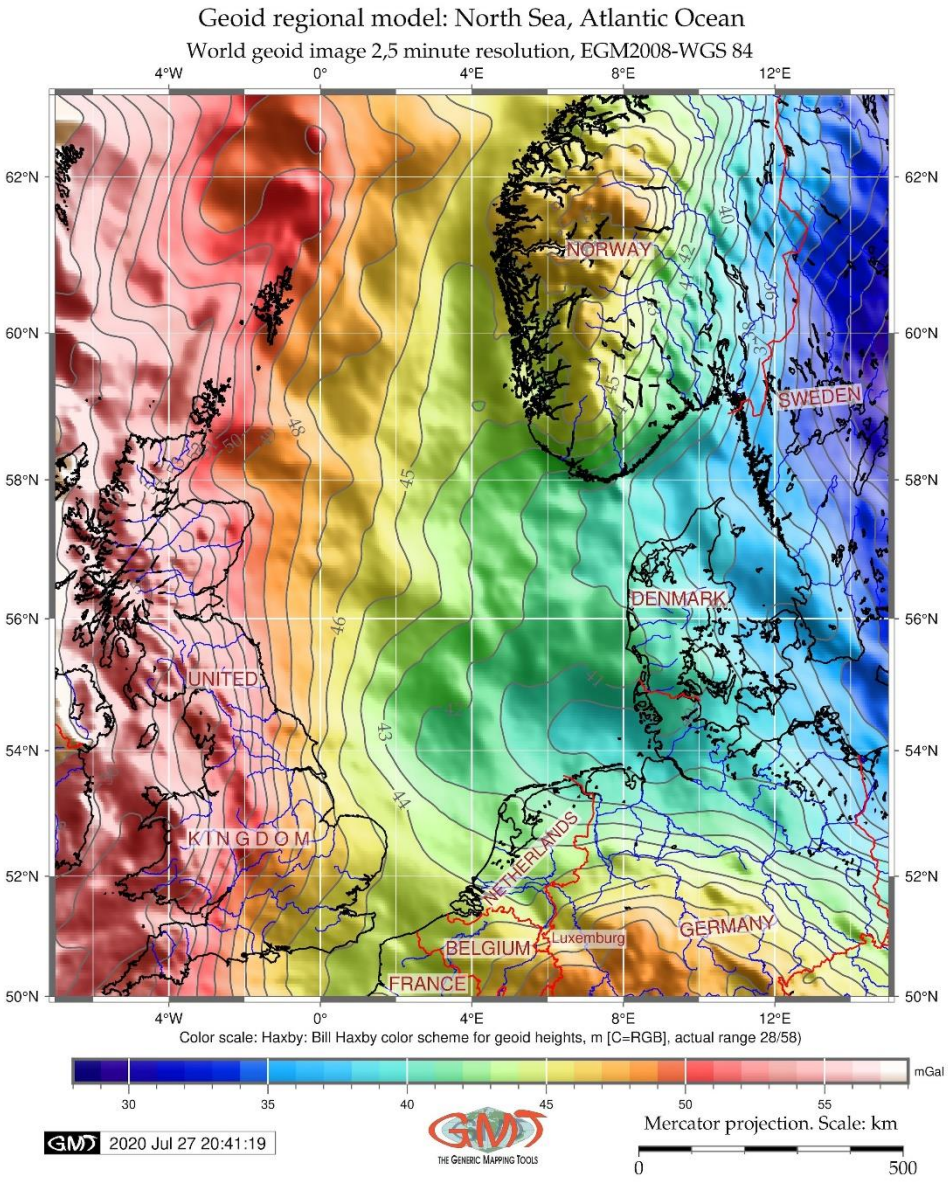

Figure 3. Geoid model of the North Sea basin. Source: author.

The undersea feature names and text annotations were controlled by the existing Gazetteer (IHO-IOC GEBCO, 2020). The coastal lines and contours were derived from the GMT-embedded crude dataset GSHHS (Global Self-consistent, Hierarchical, High-resolution Shoreline database) developed by Wessel and Smith (1996). All data have been integrated into the Generic Mapping Tools (GMT) scripting cartographic toolset and processed using methodological approach of GMT (Wessel and Smith, 1991, 1995; Wessel et al. 2013). To identify the sediment thickness diversity over the North Sea basin, the visualized dataset of sediment thickness was compared against the marine free-air gravity, geoid and topography maps using GMT version 6.0.0.

The data were subset over the basin of the North Sea with a spatial extent having coordinates 7°W-15°E,50°N-63°N. The data extent was selected using GMT 'grdcut' module (grdcut GEBCO_2019.nc -R-7/15/50/63 -Gns_relief.nc). The GEBCO dataset provides an open access 15-arc-second resolution topographic grid: https://www.gebco.net/. The topographic dataset coverage is from -2273.947 (water depth) to a maximum at 2344.548 (topographic elevations), as checked up by GDAL (GDAL/OGR contributors 2020): gdalinfo ns_relief.nc -stats. The dataset of the geoid model Earth Gravitational Model of 2008 (EGM2008) shows the geoid undulations over the North Sea basin. It has a 2,5 min spatial resolution, datum WGS-1984. The EGM2008 was developed using the GRACE data and a global dataset of the terrestrial gravity anomalies including both land and marine areas. The EGM2008 was released by the National Geospatial-Intelligence Agency (NGA) EGM Development Team 2008 as an open access data from: http://earthinfo.nga.mil/GandG/wgs84/gravitymod/egm2008/index.html

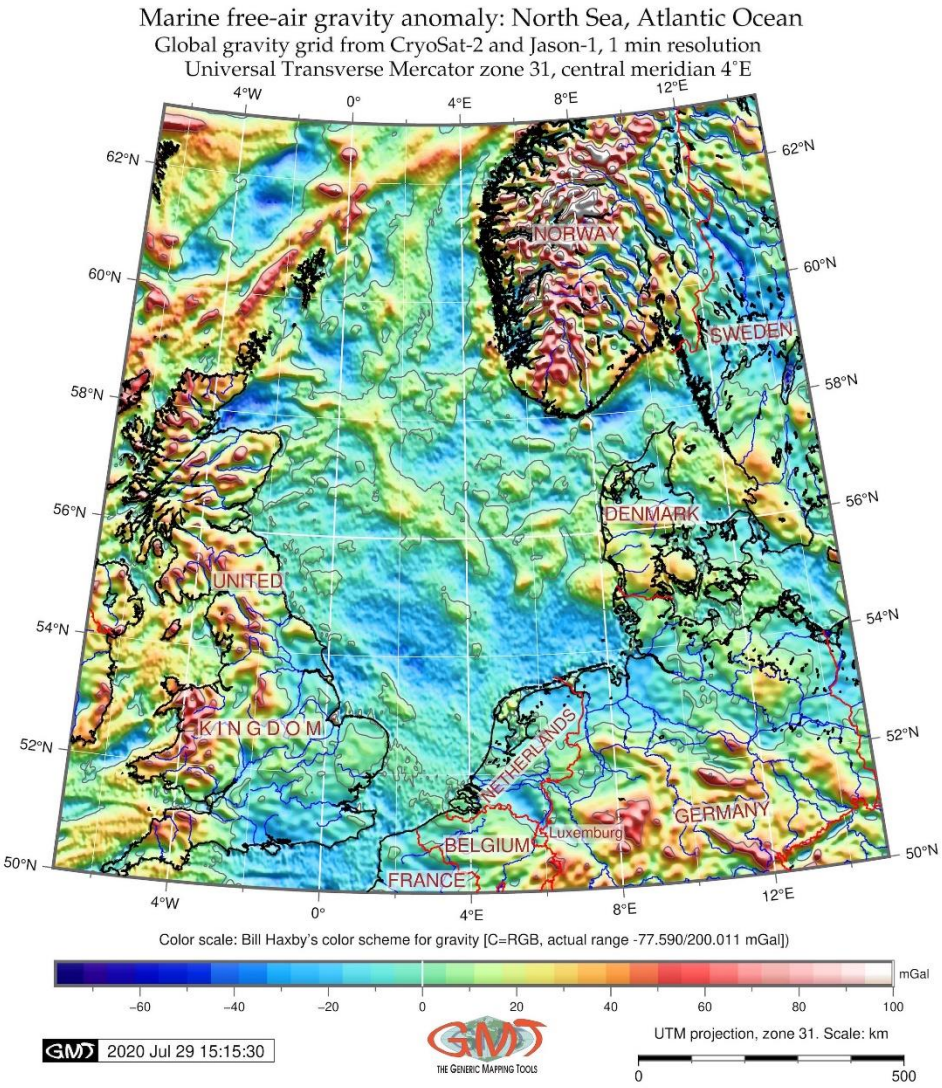

Figure 4. Marine free-air gravity map of the North Sea basin. Source: author.

A network of the seafloor covering sediment thickness data of a high-resolution GlobSed total sediment thickness in the world's oceans was collected and subset for the study area with the following statistical information on data by GDAL data inspection: extent from zero to over 12 km (maximum=12779.642), mean=3153.716, standard deviation=2564.538. The geospatial data have been processed, visualized and interpreted using GMT scripts to investigate the correlation between the geologic and geophysical settings and topography of the basin. The vector lines containing political national boundaries, rivers, coastal land/water borders have been obtained by GMT as embedded layers and added to the maps using 'pscoast' module of GMT which plots continents, shorelines, rivers, and borders on maps. The cartographic visualization was done by the GMT code: 'gmt pscoast -R -J -P -Ia/thinner,blue -Na -N1/thick,red -W0.2p -Df -O -K >> $ps' (Lemenkova, 2019b). Here, the flag '-I' stands for the river network, '-N1' – national borders, '-Na' – marine and state boundaries.

Data visualization and cartography are important for visual analysis and reading the maps, since they facilitate the mental perception of reality of the existing geographical phenomena. Therefore, the Colour Palettes Tables (cpt) were selected from the existing GMT embedded cpt individually for each map. The extent of the cpt was defined using data inspection by GDAL. For instance, the main components and content of the sediments have been visualized by means of 'Turbo' Google's Improved Rainbow Colormap for Visualization using 'makecpt' GMT module: 'gmt makecpt -Cturbo.cpt -V -T0/12779/500 > colors.cpt' (Lemenkova, 2019c). Turbo is a smooth sensible false-colour palette attracting attention through high brightness and saturation levels of colours and a hue component, suitable for sediment thickness visualizing by its contrasting and effectiveness. Here the data extent is set up from 0 to 12779 with a step of 500 which is defined by flag '-T0/12779/500'. The '-V' flag defines the level of verbosity of the GMT code.

RESULTS AND DISCUSSIONS

A multi-disciplinary data of sediment thickness, topographic and geophysical observations from the North Sea and the adjacent southern Norwegian regions was performed by GMT. The presented topographic map of the North Sea (Fig. 1) shows variations in the seafloor relief. An extensive trough with depths of up to 12 km is stretching in the central and southern parts of the North Sea. Another deep trough, the Danish-Polish Marginal Trough covers the area of the Danish straits and the southwestern part of the Baltic Sea. It also includes the adjacent coastal lowlands. The crystalline basement surface forming a stepped plateau with depths lesser than 1 km is located within the shelf to the north and west of the British Isles. Within the continental slope, it is bordered by a steep scarp slope to a wide pre-continental trough with a depth of 4-5 km, stretching along the Rockall Trough and the Faroe-Shetland sedimentary basin formed by the Mesozoic rifting. The Rockall Trough, located on the N border of the North Sea, separates the sub-continental structures of the topographically-elevated regions of Rockall Plateau, the Faroe Islands and Iceland from the continental margin. The crystalline basement is exposed in the region of the Faroe Islands, the Rockall Plateau. Here its surface is submerged to depths at about 1 km, and in the trough between the banks up to depths >2 km.

The origin, transport, dispersal and deposition of the sediments both in the open regions of the North Sea and in its highly dynamic and vulnerable coastal regions has a strong and systematic variability. As can be noted on Fig. 2, the sedimentary layers on the shelf are increasing northward towards the Arctic reaching the highest values (12779.642 m) in the SW coast of Norway. This can be explained as a result of the concept of the isostatic equilibrium. The deposition of sediments away from the ridge causes the nearby oceanic crust to sink determining isostatic re-adjustment. However, in such a case, the layers should be tilted landwards, since the largest amount of sedimentary material comes from the coast, as noted previously. If sedimentation is compensated by the deflection of the continental crust, the boundaries between the individual layers should be parallel, but they present a rather complex pattern with out-of-sequence dislocations (Fig. 2). Moderate values (5,000-6,000 m) colored as green areas on Fig. 2 stretching in NW direction in the central part of the sea clearly correlate with the marine gravity anomaly isolines with values 10-20 mGal (light green to green colored areas, Fig. 4) which points at the local relief forms of the central North Sea. The submarine geomorphology can also be seen by analyzing of the Fig. 1. The geoid undulations show range of the geoid heights in 28–58 m, and increase of values in westward direction (Great Britain area, red colors on Fig. 3).

The GlobSed covering the North Sea basin proved the latitude correlation between the topography and sediment thickness which increases toward high northern latitudes, as visualized on Fig. 2. The biochemical context of the North Sea waters correlates with the supply of the sedimentary material from the adjacent coastal land. Its southern part has an inflow of numerous rivers, while the northern part has an inflow of Atlantic waters. The rivers Elbe, Weser, Rhine, Meuse and small rivers of the eastern coast of Great Britain flow into the W and S parts of the North Sea. In its S part, the North Sea waters receive terrigenous sedimentary material from the rivers. Here the terrigenous sediments are rapidly deposited near the river mouths, depending on a geomorphic system controlling the character of sedimentation in the estuaries (Wadden See, Bay of Kiel) and on the size of the suspended matter.

The subsidence of the outer shelf and increase of sediment thickness shows the relationship with the age of the underlying oceanic lithosphere and topographic location increasing toward high southern and northern latitudes. It is also associated with the sink of the peripheral areas of the Arctic ocean caused by the submarine relief. In this case, the topographic compensation for the seafloor subsidence by increasing sediment thickness may be complete or incomplete, which explains local dislocations. The sedimentary cover is generally thin and monoclinal on the shelf areas along the coasts of Scotland and Ireland, although its thickness noticeably increases in some small depressions. Sediments from the

middle to late Eocene and during the middle to late Oligocene are located to the east and northeast of the North Sea basin. Vast basin of the North Sea is covered by the deposits from the Upper Paleozoic Era (Permian Period, ca. 300 to 250 M years), from the Mesozoic (ca. 250-66 M years) and a Cenozoic Era earlier than 66 M years according to the geological time scale (Gradstein et al. 2004). A total sediment thickness of up to 12 km, and the Cenozoic sediments are no more than 3 km. The Palaeogene uplift of Scandinavia in the eastern North Sea Basin was caused by the regional tectonic movements along crustal zones of weakness (Clausen et al., 2000). The sediment thickness is also determined by the weight of the deposited materials, similar to that near the large river deltas. It can be also explained by the movement of the ocean plates causing dislocations of the sediment.

CONCLUSIONS

The topographic conditions of the North Sea seafloor create varied conditions for the sedimentation distribution and depositions of the materials originating from adjacent lands of north European countries. The accumulation of the terrigenous materials on the North Sea seafloor is controlled by various factors. These include climatic and hydrodynamic local settings, tectonic and geologic evolution of the region, seabed bathymetry (interchange of elevations and depressions), type and size of the sediment particles, among others. Large areas of active sedimentation processes can be distinguished in the northern areas (southern Norway) where the volume of the sedimentation and the rates of the deposition are high. Thick sediment layer is notable in the trap near the Faroe Islands in the higher latitude of the North Sea, Fig. 2. In general, sediment thickness is increased in the topographic depressions, however, some areas are noted by local sediment deposition.

The process of the sedimentation in the North Sea has uneven pattern of distribution and demonstrate correlation with topographic and geophysical maps. The interplay of the geological complex processes with topography and physiographic relief landforms has been studied and reported in various papers: tectonic evolution and processes of mantle circulation and heat release (Steinberger, B. 2007; Steinberger et al. 2001), morphological evidence for the Last Glacial Maximum ice extent (Prins and Andresen, 2019), geological parameters controlling the petrophysics (Faÿ-Gomord et al. 2018), tidal motion with respect to the physical oceanography (Otto et al. 1990), geologic settings, erosion and sediment coverage controlling the modern topography, variety and distribution of the relief landforms (Lemenkova, 2018, 2020a, 2020b).

There are various approaches to evaluate sediments using direct observations and samplings. For instance, sampling Pliocene and Pleistocene marine sediments can be achieved by using piston and gravity corer devices for sediment coring and multi-corer and box corer systems to collect surface sediments (Kuhn et al. 2007). However, such direct observations and data sampling are expensive, time-consuming and require special equipment. Using advanced methods of cartographic visualization of digital datasets presents the way of studying correlations between the sediment distribution and geophysical fields. Cartography aims for the increase of precision of data visualization highlighting such correlations by the effective data presentation. Advances in cartographic automatization are published in Schenke and Lemenkova (2008). However, GMT presented further steps in machine learning methods of mapping and geological data visualization. The automatic approach of GMT presents the scripting mapping techniques which differ from the traditional GIS (Klaučo et al. 2013, 2017, Suetova et al. 2005a, 2005b; Lemenkova et al. 2012) and are similar to those of the programming languages (Lemenkova 2019d, 2019e).

Using GMT or a combination of the GMT and ESRI ArcGIS software (Gauger et al. 2007) for integration of the high-resolution multi-source data makes visualization of the geological and geophysical settings with topographic landforms more robust, direct and effective comparing to the GIS-projects requiring lots of manual manipulation with data. Correct and effective data visualization, by means of a GMT-based graphical presentation enables to draw the correct conclusions while reading the map (e.g. Lemenkova, 2020c, 2020d). The repeatability of the GMT scripts results in the flexibility of mapping process depending on the feedback, as the cartographer can evaluate the effect of the map and replot the image. In this way, the cartographic mapping based on GMT presents a cognitive process enabling to get to the essence of a geophysical phenomena. Speed of the shell scripting enables to focus on reading the map and interpreting the visualized geographical phenomena rather than cartographic techniques: inspection of geologic structures, topographic relief and its correct representation, relevant characteristics of the colour scale for gravity anomalies, data origin, resolution and quality. In case of need, the data can be replotted relatively quick using various experiments with data projections, colours, scales, visualization of the elements on maps.

REFERENCES

Alappat L., Vink A., Tsukamoto S., Frechen M. 2010. Establishing the Late Pleistocene–Holocene sedimentation boundary in the southern North Sea using OSL dating of shallow continental shelf sediments. *Proceedings of the Geologists' Association* 121 (1), pp. 43-54.

Banse K. 1956. Produktionsbiologische Serienbestimmungen im südlichen Teil der Nordsee im März 1955. *Kieler Meeresforschung* 12, pp. 166.

Clausen O. R., Nielsen O. B., Huuse M., Michelsen O. 2000. Geological indications for Palaeogene uplift in the eastern North Sea Basin. *Global and Planetary Change* 24(3–4), pp. 175-187.

de Haas H., Boer W., van Weering T.C.E. 1997. Recent sedimentation and organic carbon burial in a shelf sea: the North Sea. *Marine Geology* 144 (1–3), 131-146.

Faÿ-Gomord O., Verbiest M., Lasseur E., Caline B., Allanic C., Descamps F., Vandycke S., Swennen R. 2018. Geological and mechanical study of argillaceous North Sea chalk: Implications for the characterisation of fractured reservoirs. *Marine and Petroleum Geology* 92, pp. 962-978.

Fettweis M., Monbliu J., Baeye M., Nechad B., Van den Eynde D. 2012. Weather and climate induced spatial variability of surface suspended particulate matter concentration in the North Sea and the English Channel. *Methods in Oceanography* 3–4, pp. 25-39.

Flemming N.C., Harff J., Burgess A., Bailey G.N., Moura D. (eds.) 2017. *Submerged landscapes of the European continental shelf: Quaternary paleoenvironments* (Vol. 1). Wiley-Blackwell, Chichester, UK.

Gauger S., Kuhn G., Gohl K., Feigl T., Lemenkova P., Hillenbrand C. 2007. Swath-bathymetric mapping. *Reports on Polar and Marine Research* 557, pp. 38–45.

GEBCO Compilation Group 2020. *GEBCO 2020 Grid*. DOI: 10.5285/a29c5465-b138-234d-e053-6c86abc040b9

IHO-IOC GEBCO 2020. International Hydrographic Organization Intergovernmental Oceanographic Commission General Bathymetric Chart of the Ocean Gazetteer of Undersea Feature Names. http://www.gebco.net/data_and_products/undersea_feature_names/

GDAL/OGR contributors 2020. *GDAL/OGR Geospatial Data Abstraction software Library*. Open Source Geospatial Foundation. https://gdal.org.

Gradstein F. M., Ogg J. G., Smith A. G. 2004. *A Geologic Time Scale 2004*. Cambridge: Cambridge University Press.

Hache I., Karius V., Gutkuhn J., Eynatten H. 2019. The development and application of an autonomous working turbidity measurement network: Assessing the spatial and temporal distribution of suspended particulate matter on tidal flats in the North Frisian Wadden Sea. *Continental Shelf Research* 176, pp. 36-50.

Heim S., Lutz R., Nelskamp S., Verweij H., Kaufmann D., Reinhardt L. 2013. Geological Evolution of the North Sea: Cross-border Basin Modeling Study on the Schillground High. *Energy Procedia* 40, pp. 222–231.

Johnson H. D., MacKay T. A., Stewart D. J. 1986. The Fulmar Oil-field (Central North Sea): geological aspects of its discovery, appraisal and development. *Marine and Petroleum Geology* 3(2), pp. 99-125.

Klaučo M., Gregorová B., Stankov U., Marković V., Lemenkova P. 2013. Determination of ecological significance based on geostatistical assessment: a case study from the Slovak Natura 2000 protected area. *Central European Journal of Geosciences*, 5(1), pp. 28–42.

Klaučo M., Gregorová B., Stankov U., Marković V., Lemenkova P. 2017. Land planning as a support for sustainable development based on tourism: A case study of Slovak Rural Region. *Environmental Engineering and Management Journal*, 2(16), pp. 449–458.

Krey J. 1952. Untersuchungen zum Sestongehalt des Meerwassers. I. Der Sestongehalt in der westlichen Ostsee und unter Helgoland. *Berichte der Deutschen wissenschaftlichen Kommission für Meeresforschung N. F.* 12, pp. 431–456.

Krey J. 1961. Der Detritus im Meer. *Journal du Conseil Permanent International pour l'Exploration de la Mer* 26 (3), pp. 263–280.

Kuhn G., Hass C., Kober M., Petitat M., Feigl T., Hillenbrand C. D., Kruger S., Forwick M., Gauger S., Lemenkova P. 2006. The response of quaternary climatic cycles in the South-East Pacific: development of the opal belt and dynamics behavior of the West Antarctic ice sheet. In: Gohl, K. (ed). *Expeditionsprogramm Nr. 75 ANT XXIII/4, AWI*.

Laban C. 2006. Seabed mapping in the Dutch sector of the North Sea. *Sea Technology* 47, pp. 47-51.

Lekens W.A.H., Haflidason H., Sejrup H.P., Nygard A., Richter T., Vogt C., Frederichs T. 2009. Sedimentation history of the northern North Sea Margin during the last 150 ka. *Quaternary Science Reviews* 28 (5–6), pp. 469-483.

Lemenkova P. 2020a. Variations in the bathymetry and bottom morphology of the Izu-Bonin Trench modelled by GMT. *Bulletin of Geography. Physical Geography Series* 18 (1), pp. 41–60.
Lemenkova P. 2020b. GMT Based Comparative Geomorphological Analysis of the Vityaz and Vanuatu Trenches, Fiji Basin. *Geodetski List*, 74 (1), pp. 19–39.
Lemenkova P. 2020c. Visualization of the geophysical settings in the Philippine Sea margins by means of GMT and ISC data. *Central European Journal of Geography and Sustainable Development* 2 (1), pp. 5–15.
Lemenkova P. 2020d. GMT-based geological mapping and assessment of the bathymetric variations of the Kuril-Kamchatka Trench, Pacific Ocean. *Natural and Engineering Sciences* 5(1), 1–17.
Lemenkova P. 2019a. Statistical Analysis of the Mariana Trench Geomorphology Using R Programming Language. *Geodesy and Cartography* 45 (2), pp. 57–84.
Lemenkova P. 2019b. Topographic surface modelling using raster grid datasets by GMT: example of the Kuril-Kamchatka Trench, Pacific Ocean. *Reports on Geodesy and Geoinformatics* 108, pp. 9–22.
Lemenkova P. 2019c. GMT Based Comparative Analysis and Geomorphological Mapping of the Kermadec and Tonga Trenches, Southwest Pacific Ocean. *Geographia Technica* 14(2), pp. 39–48.
Lemenkova P. 2019d. AWK and GNU Octave Programming Languages Integrated with Generic Mapping Tools for Geomorphological Analysis. *GeoScience Engineering*, 65 (4), 1–22.
Lemenkova P. 2019e. Testing Linear Regressions by StatsModel Library of Python for Oceanological Data Interpretation. *Aquatic Sciences and Engineering*, 34, 51–60.
Lemenkova P. 2018. R scripting libraries for comparative analysis of the correlation methods to identify factors affecting Mariana Trench formation. *Journal of Marine Technology and Environment* 2, pp. 35–42.
Lemenkova P., Promper C., Glade T. 2012. Economic Assessment of Landslide Risk for the Waidhofen a.d. Ybbs Region, Alpine Foreland, Lower Austria. In Eberhardt, E., Froese, C., Turner, A. K., Leroueil, S. eds. Protecting Society through Improved Understanding. 11th International Symposium on Landslides and the 2nd North American Symposium on Landslides and Engineered Slopes (NASL), Banff, Canada, pp. 279–285.
Lemenkova P. 2011. *Seagrass Mapping and Monitoring Along the Coasts of Crete, Greece*. M.Sc. Thesis. University of Twente, the Netherlands.
Lindgreen H., Jakobsen F. 2012. Marine sedimentation of nano-quartz forming flint in North Sea Danian chalk. *Marine and Petroleum Geology* 38 (1), pp. 73-82.
Lyngsie S. B., Thybo H., Rasmussen T. M. 2006. Regional geological and tectonic structures of the North Sea area from potential field modelling. *Tectonophysics* 413 (3–4), pp. 147-170.
Ottesen D., Stewart M., Brönnera, M., Batchelor C. L. 2020: Tunnel valleys of the central and northern North Sea (56°N to 62°N): Distribution and characteristics. *Marine Geology* 425, 106199.
Ottesen D., Batchelor C.L., Dowdeswell J.A., Løseth H. 2018. Morphology and pattern of Quaternary sedimentation in the North Sea Basin (52–62°N). *Marine and Petroleum Geology* 98, 836-859.
Otto L., Zimmerman J.T.F., Furnes G.K., Mork M., Saetre R., Becker G. 1990. Review of the physical oceanography of the North Sea. *Netherlands Journal of Sea Research* 26 (2–4), pp. 161–238.
Pavlis N. K., Holmes S. A., Kenyon S. C., Factor J. K. 2012. The development and evaluation of the Earth Gravitational Model 2008 (EGM2008). *Journal of Geophysical Research* 117, pp. B04406.
Postma H. 1961. Suspended matter and Secchi disc visibility in coastal waters. *Netherlands Journal of Sea Research* 1 (3), pp. 359-390.
Prins L. T., Andresen K. J. 2019. Buried late Quaternary channel systems in the Danish North Sea – Genesis and geological evolution. *Quaternary Science Reviews* 223, pp. 105943.
Sadeghi S.H., Dashtpagerdi M.M., Rekabdarkoolai H.M., Schoorl J.M. 2019. Accuracy of sedimentgraph modeling from topography map scale and DEM mesh size. International Soil and Water Conservation Research 7, 138–149.
Sandwell D. T., Müller R. D., Smith W. H. F., Garcia E., Francis R. 2014. New global marine gravity model from CryoSat-2 and Jason-1 reveals buried tectonic structure. Science 346 (6205), pp. 65-67.
Schenke H. W., Lemenkova P. 2008. Zur Frage der Meeresboden-Kartographie: Die Nutzung von AutoTrace Digitizer für die Vektorisierung der Bathymetrischen Daten in der Petschora-See. *Hydrographische Nachrichten*, 81, pp. 16–21.
Smith W. H. F. 1993. On the accuracy of digital bathymetric data. *Journal of Geophysical Research* 98, B6, pp. 9591–9603.

Steinberger B. 2007. Effects of latent heat release at phase boundaries on flow in the Earth's mantle, phase boundary topography and dynamic topography at the Earth's surface. *Physics of the Earth and Planetary Interiors* 164, pp. 2-20.

Steinberger B., Schmeling H., Marquart G. 2001. Large-scale lithospheric stress field and topography induced by global mantle circulation. *Earth and Planetary Science Letters* 186, pp. 75-91.

Straume E. O., Gaina C., Medvedev S., Hochmuth K., Gohl K., Whittaker J. M., Abdul Fattah R., Doornenbal J. C., Hopper J. R. 2019. GlobSed: Updated total sediment thickness in the world's oceans. *Geochemistry, Geophysics, Geosystems*, pp. 20.

Suetova I. A., Ushakova L. A., Lemenkova P. 2005a. Geoinformation mapping of the Barents and Pechora Seas. *Geography and Natural Resources* 4, pp. 138–142.

Suetova I. A., Ushakova L. A., Lemenkova P. 2005b. Geoecological Mapping of the Barents Sea Using GIS. *International Cartographic Conference (ICC)*. 2005, La Coruna, Spain.

Swindles G. T., Galloway J. M., Macumber A. L., Croudace I. W., Emery A. R., Woulds C., Bateman M. D., Parry L., Jones J. M., Selby K., Rushby G. T., Baird A. J., Woodroffe S. A., Barlow N. L. M. 2018. Sedimentary records of coastal storm surges: Evidence of the 1953 North Sea T event. *Marine Geology* 403, pp. 262–270.

Van der Molen A. S. 2004. *Sedimentary development, seismic stratigraphy and burial compaction of the Chalk Group in the Netherlands North Sea area*. Thesis. University Utrecht, pp. 175.

van Dijk T.A.G.P., van Dalfsen J.A., van Lancker V., van Overmeeren R.A., van Heteren S., Doornenbal P.J. 2012. *Benthic habitat variations over tidal ridges, North Sea, the Netherlands.* In: Harris, P.T., & Baker, E.K. (Eds.) Seafloor Geomorphology as Benthic Habitat: GeoHAB Atlas of Seafloor Geomorphic Features and Benthic Habitats. pp. 241-249. Elsevier, Am- sterdam, the Netherlands.

Vandermarken T., Gao Y., Baeyens W., Denison M. S., Croes K. 2018. Dioxins, furans and dioxin-like PCBs in sediment samples and suspended particulate matter from the Scheldt estuary and the North Sea Coast: Comparison of CALUX concentration levels in historical and recent samples. *Science of The Total Environment* 626, pp. 109-116.

Visser, M.P. 1970. The turbidity of the southern North Sea. Deutsche Hydrographische Zeitschrift 23, pp. 97–117.

Wessel P., Smith W. H. F. 1991. Free software helps map and display data. *Eos Transactions of the American Geophysical Union* 72 (41), pp. 441.

Wessel P., Smith W. H. F. 1995. New version of the Generic Mapping Tools released. *Eos Transactions of the American Geophysical Union* 76 (33), pp. 329.

Wessel P., Smith W. H. F. 1996. A Global Self-consistent, Hierarchical, High-resolution Shoreline Database. *Journal of Geophysical Research* 101, pp. 8741-8743.

Wessel P., Smith W. H. F., Scharroo R., Luis J. F., Wobbe F. 2013. Generic mapping tools: Improved version released. *Eos Transactions American Geophysical Union* 94 (45), pp. 409–410.

Received: 29.07.2020
Revised: 31.07.2020